Supporting information

Understanding three-body contributions to coarse-grained force fields

Christoph Scherer[1, a)] and Denis Andrienko[1, b)]
Max Planck Institute for Polymer Research, Ackermannweg 10, 55128 Mainz, Germany

I. METHODS

In, the following we explain the methods used in this work, as far as they are not already described in detail in the main text in section 2.

A. Force matching (FM)

The force matching procedure has been described in the main text (subsection 2.2) including the set of linear equations. After solving the set of linear equations with a constrained least-squares solver, the CG interaction potentials are determined from the CG forces by numerical integration. Before integration, the tabulated two-body forces are multiplied by an analytic function of the form:

$$f_{\text{switch}}(r) = \cos\left(\frac{\pi}{2}\frac{r - r_{\text{sm}}}{r_{\text{cut}} - r_{\text{sm}}}\right). \tag{I.1}$$

This is done for all distances greater than $r_{\text{sm}} = 1.0$ to ensure a smooth decay to zero at the short-range cutoff of $r_{\text{cut}} = 1.2\,\text{nm}$.

B. Extension of the VOTCA-CSG FM routine to include three-body interactions

As described in the main text, we extend the VOTCA-CSG FM routine in order to complement the two-body CG interactions with three-body interactions of the Stillinger-Weber (SW) form:

$$U^{\text{SW}} = \sum_{i,j\neq i,k>j} f^{(3b)}(\theta_{ijk}) \exp\left(\frac{\gamma_{ij}\sigma_{ij}}{r_{ij} - a_{ij}\sigma_{ij}}\right) \exp\left(\frac{\gamma_{ik}\sigma_{ik}}{r_{ik} - a_{ik}\sigma_{ik}}\right). \tag{I.2}$$

In this notation, i is the index of the central atom and j and k are the other two atom indices of a triplet of atoms with an angular interaction term $f^{(3b)}(\theta_{ijk})$. To obtain the set of linear equations (eq. (4) of the main text), one has to calculate the force $\boldsymbol{f}_i^{\text{SW}} = -\nabla_i U^{SW}$ resulting from the SW interaction on each CG bead i, namely:

$$\begin{aligned}\boldsymbol{f}_i^{\text{SW}} = &\left(\frac{\partial}{\partial\theta} f^{(3b)}(\theta)\right)(-\nabla_i\theta) \exp\left(\frac{\gamma_{ij}\sigma_{ij}}{r_{ij} - a_{ij}\sigma_{ij}}\right) \exp\left(\frac{\gamma_{ik}\sigma_{ik}}{r_{ik} - a_{ik}\sigma_{ik}}\right) \\ &+ f^{(3b)}\left[(-\nabla_i r_{ij})\left(-\frac{\gamma_{ij}\sigma_{ij}}{(r_{ij} - a_{ij}\sigma_{ij})^2}\right) \exp\left(\frac{\gamma_{ij}\sigma_{ij}}{r_{ij} - a_{ij}\sigma_{ij}}\right) \exp\left(\frac{\gamma_{ik}\sigma_{ik}}{r_{ik} - a_{ik}\sigma_{ik}}\right)\right. \\ &\left.+ (-\nabla_i r_{ik})\left(-\frac{\gamma_{ik}\sigma_{ik}}{(r_{ik} - a_{ik}\sigma_{ik})^2}\right) \exp\left(\frac{\gamma_{ij}\sigma_{ij}}{r_{ij} - a_{ij}\sigma_{ij}}\right) \exp\left(\frac{\gamma_{ik}\sigma_{ik}}{r_{ik} - a_{ik}\sigma_{ik}}\right)\right],\end{aligned} \tag{I.3}$$

a) Electronic mail: scherer@mpip-mainz.mpg.de
b) Electronic mail: denis.andrienko@mpip-mainz.mpg.de

$$\begin{aligned}\boldsymbol{f}_j^{\mathrm{SW}} = &\left(\frac{\partial}{\partial\theta} f^{(3b)}(\theta)\right)(-\nabla_j\theta)\exp\left(\frac{\gamma_{ij}\sigma_{ij}}{r_{ij}-a_{ij}\sigma_{ij}}\right)\exp\left(\frac{\gamma_{ik}\sigma_{ik}}{r_{ik}-a_{ik}\sigma_{ik}}\right)\\ &+ f^{(3b)}\left[(-\nabla_j r_{ij})\left(-\frac{\gamma_{ij}\sigma_{ij}}{(r_{ij}-a_{ij}\sigma_{ij})^2}\right)\exp\left(\frac{\gamma_{ij}\sigma_{ij}}{r_{ij}-a_{ij}\sigma_{ij}}\right)\exp\left(\frac{\gamma_{ik}\sigma_{ik}}{r_{ik}-a_{ik}\sigma_{ik}}\right)\right],\end{aligned} \tag{I.4}$$

$$\begin{aligned}\boldsymbol{f}_k^{\mathrm{SW}} = &\left(\frac{\partial}{\partial\theta} f^{(3b)}(\theta)\right)(-\nabla_k\theta)\exp\left(\frac{\gamma_{ij}\sigma_{ij}}{r_{ij}-a_{ij}\sigma_{ij}}\right)\exp\left(\frac{\gamma_{ik}\sigma_{ik}}{r_{ik}-a_{ik}\sigma_{ik}}\right)\\ &+ f^{(3b)}\left[(-\nabla_k r_{ij})\left(-\frac{\gamma_{ik}\sigma_{ik}}{(r_{ik}-a_{ik}\sigma_{ik})^2}\right)\exp\left(\frac{\gamma_{ij}\sigma_{ij}}{r_{ij}-a_{ij}\sigma_{ij}}\right)\exp\left(\frac{\gamma_{ik}\sigma_{ik}}{r_{ik}-a_{ik}\sigma_{ik}}\right)\right].\end{aligned} \tag{I.5}$$

As stated in the main text (subsection 2.3), we represent $f^{(3b)}(\theta)$ with cubic splines with $g_1,\ldots,g_M$, $M = 2\,K$ spline coefficients (when using K grid points) in the same way as the representation of the two-body force field basis functions. The derivative $\frac{\partial}{\partial\theta} f^{(3b)}(\theta)$ is the analytical derivative of the cubic spline implementation, meaning the derivative is represented by a 2nd order polynomial. To obtain a linear set of equations, all terms in eqns. (I.3) to (I.5) except $f^{(3b)}(\theta)$ and $\frac{\partial}{\partial\theta} f^{(3b)}(\theta)$ are treated as prefactors. This implies that the remaining coefficients of the SW potential (eq. (I.2)), a_{ij}, a_{ik}, σ_{ij}, σ_{ik}, γ_{ij}, and γ_{ik}, have to be set beforehand. The procedure is described in the main text in subsection 2.3. This allows to include eqns. (I.3) to (I.5) into the set of linear equations (eq. (4) of the main text) which is solved by a constrained least-squares solver.

In contrast to the spline representation of the pair forces, the system of equations now includes $f^{(3b)}(\theta)$ and $\frac{\partial}{\partial\theta} f^{(3b)}(\theta)$, due to application of the chain rule when calculating the derivative of U^{SW} (see eq. (I.2)). This implies that in this case the set of spline coefficients determines $f^{(3b)}(\theta)$ and $\frac{\partial}{\partial\theta} f^{(3b)}(\theta)$ simultaneously and no numerical integration is needed.

C. Enthalpy of vaporization

In the main text, we compare the total pressures and enthalpies of vaporization of the atomistic and the CG simulations to experimental values. All pressures refer to the virial pressures including all two-body, three-body and electrostatic long-range interactions.[1]

The molar enthalpies of vaporization ΔH or, in other words, the enthalpy differences between the gas phase and the liquid phase are calculated according to the formulation in Refs. 2 and 3:

$$\Delta H = H_{\mathrm{gas}} - H_{\mathrm{liq}} = \langle E_{\mathrm{int,gas}} + p_{\mathrm{gas}}V_{\mathrm{gas}}\rangle - \langle E_{\mathrm{int,liq}} + p_{\mathrm{liq}}V_{\mathrm{liq}}\rangle = \langle E_{\mathrm{pot,gas}}\rangle + RT - \langle E_{\mathrm{pot,liq}} + p_{\mathrm{liq}}V_{\mathrm{liq}}\rangle\,. \tag{I.6}$$

The internal energies, $E_{\mathrm{int,gas}} = E_{\mathrm{pot,gas}} + E_{\mathrm{kin,gas}}$ and $E_{\mathrm{int,liq}} = E_{\mathrm{pot,liq}} + E_{\mathrm{kin,liq}}$, refer to the total internal energies of the liquid phase and the gas phase, normalized to one molecule. As we consider the liquid state and the gas state at the same temperature ($T = 300\,\mathrm{K}$), the average kinetic energies $\langle E_{\mathrm{kin,gas}}\rangle$ and $\langle E_{\mathrm{kin,liq}}\rangle$ cancel out and only the difference of the average total potential (cohesive) energies is relevant: $\langle E_{\mathrm{pot,gas}}\rangle - \langle E_{\mathrm{pot,liq}}\rangle$ (see eq. (I.6)). In principle, both, consist of inter- and intra-molecular contributions E_{inter} and E_{intra}. In case of the all-atom simulations, we determine $E_{\mathrm{pot,gas}}$ with gas phase simulations at $T = 300\,\mathrm{K}$ with one single molecule in a simulation box of $L_{box} = 10\,\mathrm{nm}$ (see Ref. 2). In doing so, we assume that there is no inter-molecular contribution to the gas phase potential energy: $E_{\mathrm{pot,gas}} \simeq E_{\mathrm{intra,gas}}$. In case of a single bead CG representation as used in this work, there is no intra-molecular potential energy in the gas phase at all and the total potential energy of the gas phase is assumed to be $E_{\mathrm{pot,gas}} \simeq E_{\mathrm{intra,gas}} \simeq 0$. This means, we assume the CG gas to be an ideal gas (following the argumentation in Ref. 3) with a total enthalpy of $H_{\mathrm{gas}} = 2.5\,RT$ with $1.5\,RT$ attributed to the (canceled out) kinetic energy $E_{\mathrm{kin,gas}}$ and $1.0\,RT$ attributed to $\langle p_{\mathrm{gas}}V_{\mathrm{gas}} = RT\rangle$ (equation of state of an ideal gas). In the case of the all-atom NVT MD simulations, the average liquid pressure is basically equal to zero: $p_{\mathrm{liq}} = 1\,\mathrm{bar} \simeq 0$. Therefore, the term $\langle p_{\mathrm{liq}}V_{\mathrm{liq}}\rangle$ can be neglected when evaluating eq. (I.6). In case of the CG NVT MD simulations (which are conducted at the atomistic density), we have to explicitly evaluate $\langle p_{\mathrm{liq}}V_{\mathrm{liq}}\rangle$.

II. LENNARD JONES TEST SYSTEM

In the following, we introduce a single component Lennard-Jones (LJ) test system to verify the correctness of our FM parametrization scheme. We do this to clarify that the development of a short-range attraction upon including the

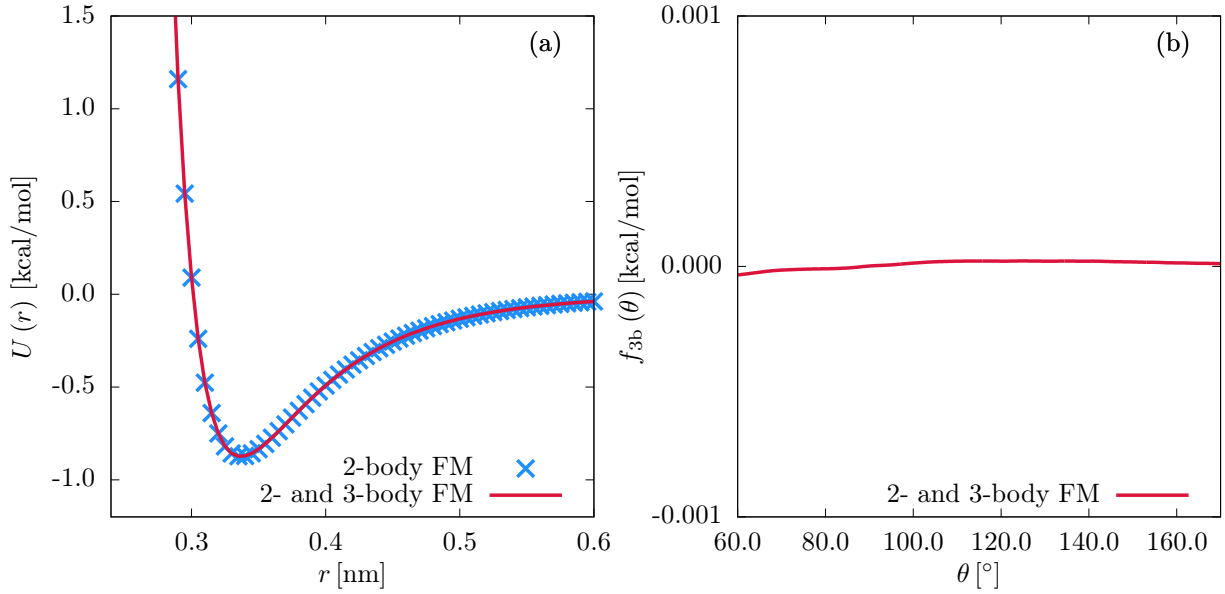

FIG. 1. (a) Pair potentials and (b) angular interaction term $f^{(3b)}\left(\theta_{ijk}\right)$ of the SW three-body potential (I.2) for the two-body only (2-body FM) and two- and three-body (2- and 3-body FM) parametrization of the LJ test system with a one-to-one CG mapping scheme.

three-body potential (see Fig. 2(a) for water and 5(a) for methanol) is not purely a numerical effect. The simulation details are as follows: We simulate a 1000 atom single component LJ system,

$$U^{\mathrm{LJ}} = 4\,\epsilon\,\left[\left(\frac{\sigma}{r}\right)^{12} - \left(\frac{\sigma}{r}\right)^{6}\right], \tag{II.1}$$

with $\epsilon = 1.0\,\mathrm{kcal/mol}$, $\sigma = 0.3\,\mathrm{nm}$ and a cutoff of 1.2 nm. We use the LAMMPS package.[4] We employ a time step of 2 fs and a chain of three Nose-Hoover thermostats[5,6] with a damping parameter of 200 fs when integrating the equations of motion.[7] We first conduct a NPT equilibration run of 20 ns with an additional chain of three Nose-Hoover barostats with a damping parameter of 1000 fs. This is followed by a 20 ns production run at the average density of the preceding NPT simulation, resulting in a box length of $L_{\mathrm{Box}} = 3.13951\,\mathrm{nm}$.

The CG procedure and the CG two-body and three-body SW potentials are described, in detail, in subsections II.B. and II.C. of the main text and subsections I A and I B of the supporting information. Here, we apply a cutoff of $r_{\mathrm{c}} = 1.2\,\mathrm{nm}$ for the pair interactions and $a = 0.46\,\mathrm{nm}$, $\sigma = 1.0$, and $\gamma = 0.08\,\mathrm{nm}$ for the three-body SW parametrization. We perform two different parametrizations. In all cases, we apply a one-to-one CG mapping scheme. First, we do FM with two-body interactions only (2-body FM). Second, we perform an unconstrained FM parametrization of two- and three-body interactions together (2-body and 3-body FM).

The results are shown in Fig. 1. One can clearly see that in this test case the pair potentials of the two different parametrization schemes coincide. They correspond exactly to the input LJ potential. The three-body interaction term of the two- and three-body optimization $f^{(3b)}\left(\theta_{ijk}\right)$ is equal to zero within statistical noise. This confirms the numerical correctness of the FM parametrization scheme, as in this test case no higher-order interactions are present.

III. ADDITIONAL STRUCTURAL PROPERTIES

In the following, we show CG potentials, distribution functions, and potentials of means force (PMFs) that are not shown in the main text. All these plots refer to the optimal SW interaction parameter of $\gamma = 0.08\,\mathrm{nm}$. In addition, we show the average angles between two-body and three-body force components on each CG bead.

A. Liquid water

In this subsection, we provide additional information on liquid SPC/E water.

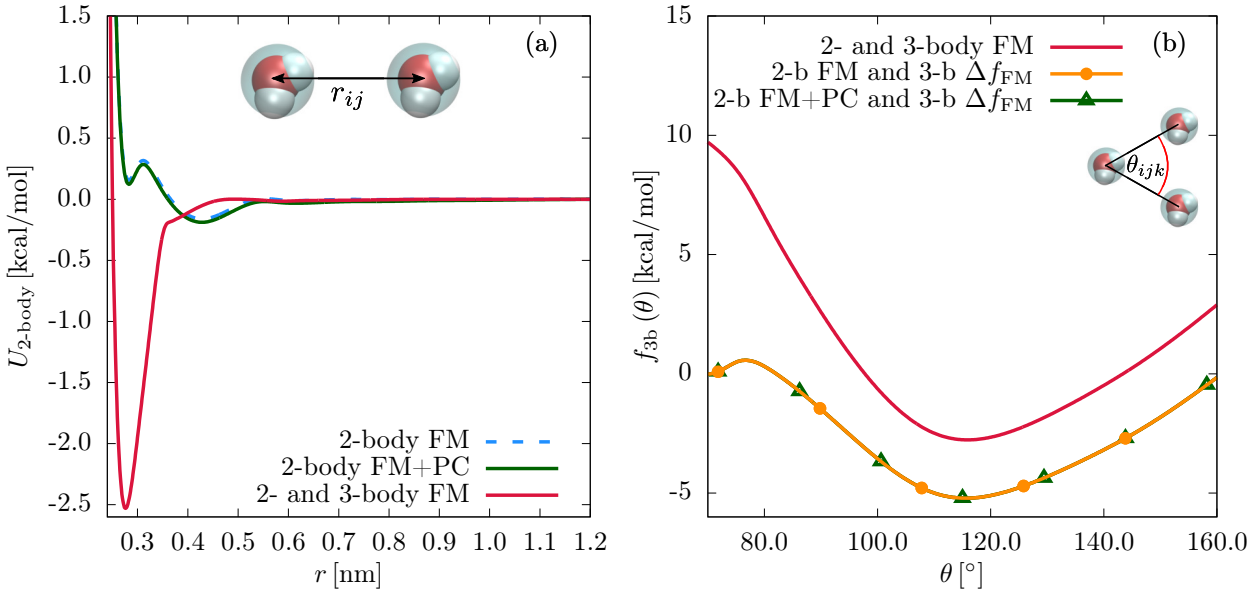

FIG. 2. (a) Pair potentials and (b) tabulated angular interaction terms $f^{(3b)}(\theta_{ijk})$ of the SW three-body potential (I.2) for CG SPC/E water for all different parametrizations.

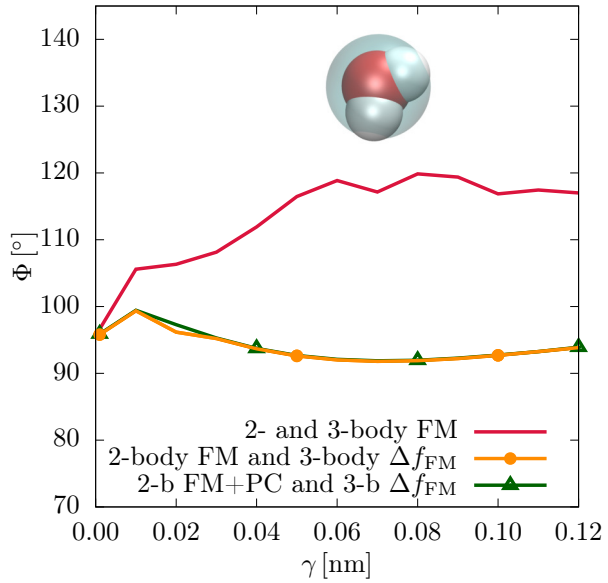

FIG. 3. Average angles $\bar{\Phi}$ between the two-body and three-body force components on each CG bead according to eqns. (7), and (8) of the main text for different CG parametrization schemes for SPC/E water. The results shown are for the concurrent two-body and three-body FM parametrization (2- and 3-body FM), the three-body FM using the residual force of the two-body FM potential (2-body FM and 3-body Δf_{FM}), and the three-body FM parametrization using the residual force of the two-body FM potential with additional pressure correction (2-b FM+PC and 3-b Δf_{FM}).

In Fig. 2(a), we show all different pair potentials for liquid SPC/E water. It complements Fig.1(a) of the main text by showing the full interaction range until the two-body cutoff radius of 1.2 nm. The first curve refers to the two-body parametrization (2-body FM). The second curve shows the two-body force matching result with pressure correction (2-body FM+PC). The pressure correction referes to the simulation of the two-body FM potential together with the three-body potential parametrized according to the residual force (2-body FM+PC and 3-body Δf_{FM}). The third curve shows the two-body part of the concurrent FM two- and three-body parametrization (2- and 3-body FM).

In Fig. 2(b), we show the tabulated angular part of the short-range three-body SW potential (I.2) $f^{(3b)}(\theta_{ijk})$ for all different CG parametrizations. One can clearly see that the parametrization according to the residual force

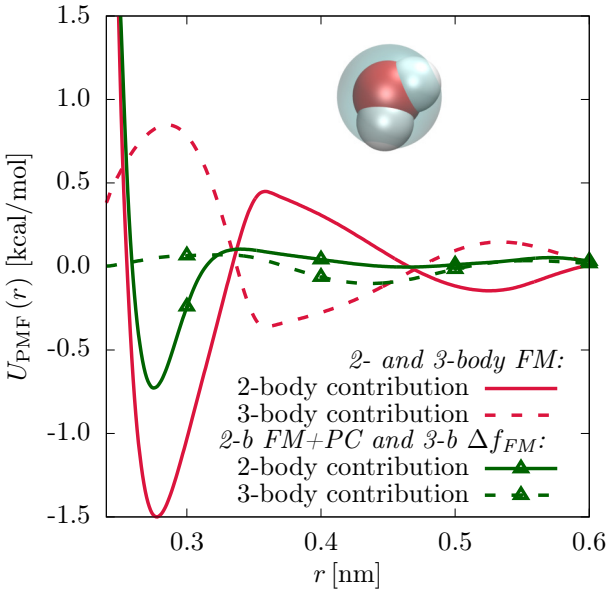

FIG. 4. Decomposition of the CG two-body PMF for different CG parametrization schemes for SPC/E water. The results shown are for the concurrent two-body and three-body FM parametrization (2- and 3-body FM), and the three-body FM using the residual force of the two-body FM potential with additional pressure correction (2-body FM+PC and 3-body Δf_{FM}).

(2-body FM and 3-body Δf_{FM}) mainly leads to a vertical shift of $f^{(3b)}(\theta)$ compared to the concurrent two-body and three-body CG parametrization (2- and 3-body FM). The angular part of the parametrization including pressure correction (2-body FM+PC and 3-body Δf_{FM}) corresponds to the uncorrected one (2-body FM and 3-body Δf_{FM}), as the pressure correction is only applied to the two-body FM potential.

In Fig. 3, we show the average angle $\bar{\Phi}$ corresponding to the inner product p of the different force field contributions (see eqns.(7), (8) of the main text). This corresponds to the average angle on each CG bead between the two-body and three-body SW force components. We show the results for varying SW interaction parameter γ (see eqn. (I.2)) for the concurrent two-body and three-body FM parametrization (2- and 3-body FM), the three-body FM using the residual force of the two-body FM potential (2-body FM and 3-body Δf_{FM}), and the three-body FM parametrization using the residual force of the two-body FM potential with additional pressure correction (2-b FM+PC and 3-b Δf_{FM}).

In Fig. 4, we show the splitting of the total two-body PMF into the two-body and three-body contributions for SPC/E water. Here, the splitting of the parametrization using the residual force of the two-body FM potential with additional pressure correction (2-body FM+PC and 3-body Δf_{IBI}) is compared to the concurrent two-body and three-body parametrization (2-body and 3-body FM). This complements Fig.4(a) of the main text. One can clearly see that the pressure correction does not change the results of the residual force parametrization without the correction.

B. Liquid methanol

In this subsection, we give additional information for liquid methanol.

In Fig. 5(a), we show all different pair potentials for liquid methanol. It complements Fig.2(a) of the main text by showing the full interaction range until the two-body cutoff radius of 1.2 nm. The first curve refers to the two-body parametrization (2-body FM). The second curve shows the two-body force matching result with pressure correction (2-body FM+PC). The pressure correction referes to the simulation of the two-body FM potential together with the three-body potential parametrized according to the residual force (2-body FM+PC and 3-body Δf_{FM}). The third curve shows the two-body part of the concurrent FM two- and three-body parametrization (2- and 3-body FM).

In Fig. 5(b), we show the tabulated angular part of the short-range three-body SW potential (I.2) $f^{(3b)}(\theta_{ijk})$ for all different CG parametrizations of liquid methanol. One can clearly see that the parametrization according to the residual force (2-body FM and 3-body Δf_{FM}) mainly leads to a vertical shift of $f^{(3b)}(\theta)$. The angular part of the parametrization including pressure correction (2-body FM+PC and 3-body Δf_{FM}) corresponds to the uncorrected one (2-body FM and 3-body Δf_{FM}), as the pressure correction is only applied to the two-body FM potential.

In Fig. 6, we show the radial distribution functions for all different CG force-fields of methanol. The two-body parametrization (2-body FM) and concurrent FM two- and three-body parametrization (2- and 3-body FM) lead to

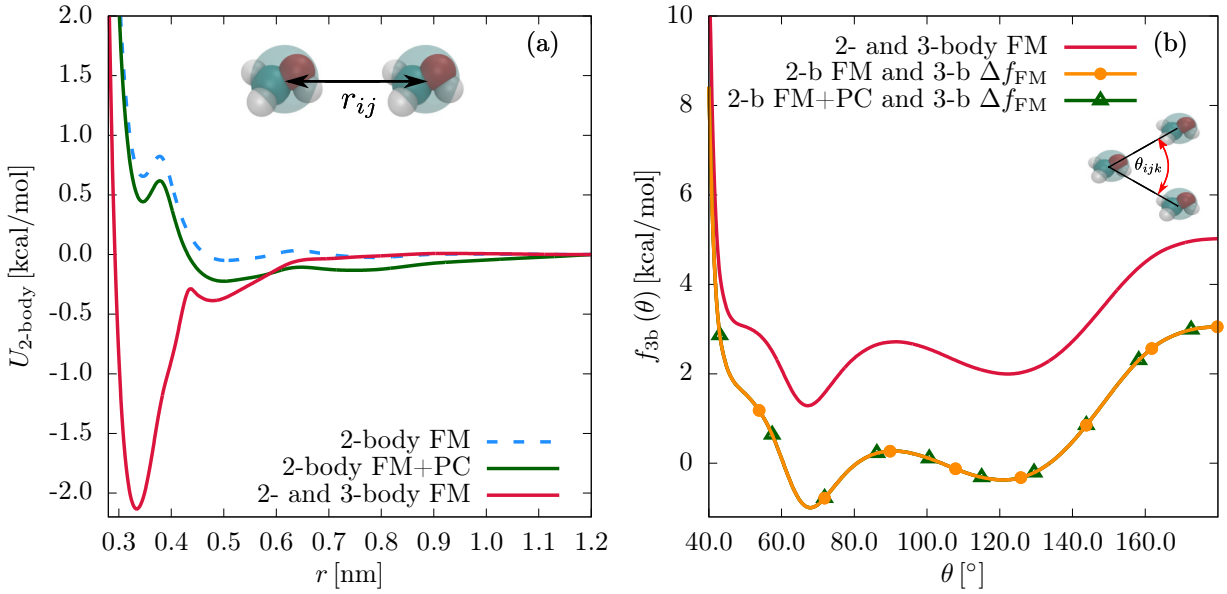

FIG. 5. (a) Pair potentials and (b) tabulated angular interaction terms $f^{(3b)}(\theta_{ijk})$ of the SW three-body potential (I.2) for CG methanol for all different parametrizations.

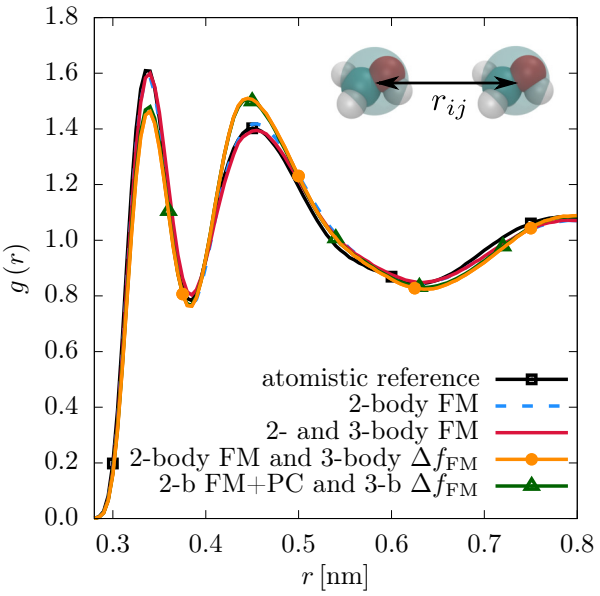

FIG. 6. Radial distribution functions of CG methanol. The different CG parametrizations refer to: FM with a (tabulated) pair potential only (2-body FM), concurrent two-body and three-body FM parametrization (2- and 3-body FM), the three-body FM parametrization using the residual force of the two-body FM potential (2-b FM and 3-b Δf_{FM}), and the three-body FM parametrization using the residual force of the two-body FM potential with additional pressure correction (2-b FM+PC and 3-b Δf_{FM}).

nearly identical results. The parametrizations of the three-body interactions according to the residual force with and without pressure correction (2-body FM and 3-body Δf_{FM}, and 2-b FM+PC and 3-b Δf_{FM}) show a slight decrease of the height of first- and increase of the second-neighbor peak compared to the atomistic reference curve. This is attributed to the short-range repulsion of the additional three-body SW potential.

In Fig. 7, we show the average angle $\bar{\Phi}$ corresponding to the inner product p of the different force field contributions (see eqns.(7), (8) of the main text). This corresponds to the average angle on each CG bead between the two-body and three-body SW force components. We show the results for varying SW interaction parameter γ (see eqn. (I.2)) for concurrent two-body and three-body FM parametrization (2- and 3-body FM), the three-body FM using the residual

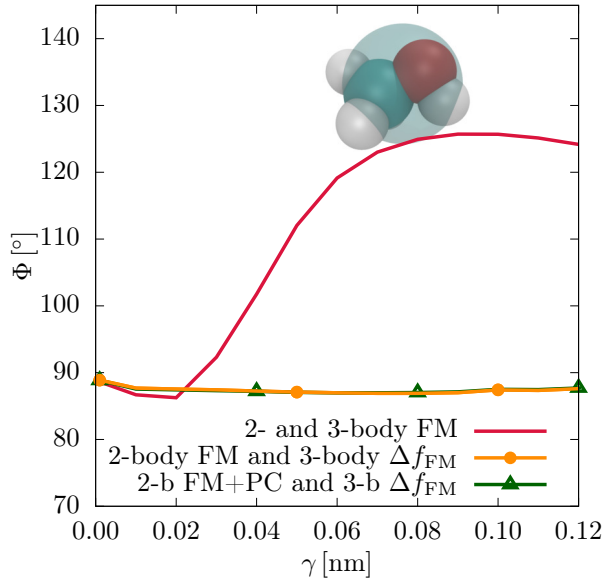

FIG. 7. Average angles $\bar{\Phi}$ between the two-body and three-body force components on each CG bead according to eqns. (7), and (8) of the main text for different CG parametrization schemes for methanol. The results shown are for the concurrent two-body and three-body FM parametrization (2- and 3-body FM), the three-body FM using the residual force of the two-body FM potential (2-body FM and 3-body Δf_{FM}), and the three-body FM parametrization using the residual force of the two-body FM potential with additional pressure correction (2-b FM+PC and 3-b Δf_{FM}).

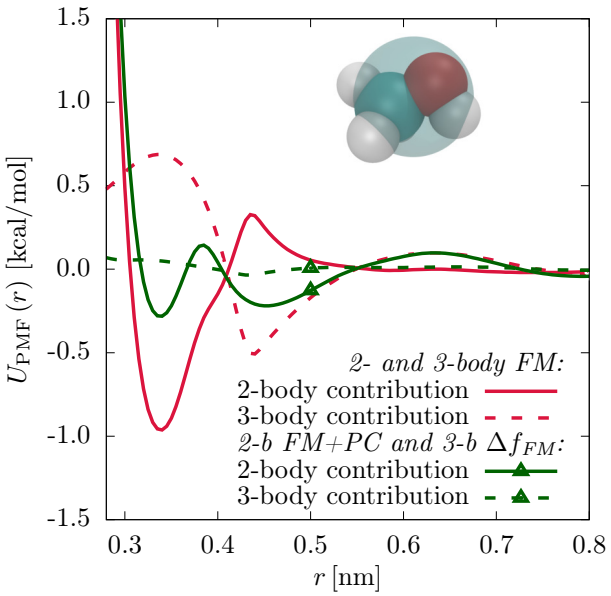

FIG. 8. Decomposition of the CG two-body PMF for different CG parametrization schemes for SPC/E water. The results shown are for the concurrent two-body and three-body FM parametrization (2- and 3-body FM), and the three-body FM using the residual force of the two-body FM potential with additional pressure correction (2-body FM+PC and 3-body Δf_{FM}).

force of the two-body FM potential (2-body FM and 3-body Δf_{FM}), and the three-body FM parametrization using the residual force of the two-body FM potential with additional pressure correction (2-b FM+PC and 3-b Δf_{FM}).

In Fig. 8, we show the splitting of the total two-body PMF into the two-body and three-body contributions for methanol. Here, the splitting of the parametrization using the residual force of the two-body FM potential with additional pressure correction (2-body FM+PC and 3-body Δf_{IBI}) is compared to the concurrent two-body and three-body parametrization (2-body and 3-body FM). This complements Fig.4(b) of the main text. One can clearly see that the pressure correction does not change the results of the residual force parametrization without the correction.

water		methanol	
γ [nm]	A [kcal/mol]	γ [nm]	A [kcal/mol]
0.001	0.107313694	0.001	0.27605193
0.01	0.103011586	0.01	0.278680996
0.02	0.087954208	0.02	0.28202708
0.03	0.072179812	0.03	0.285851176
0.04	0.059273488	0.04	0.289675272
0.05	0.050430266	0.05	0.293260362
0.06	0.045172134	0.06	0.296128434
0.07	0.043260086	0.07	0.298279488
0.08	0.043738098	0.08	0.299713524
0.09	0.046367164	0.09	0.300430542
0.10	0.05019126	0.10	0.29636744
0.11	0.055210386	0.11	0.300430542
0.12	0.060707524	0.12	0.299713524

TABLE I. Magnitudes A of the pressure corrections applied to the two-body FM potentials of CG SPC/E water and methanol for all different interaction parameters γ.

IV. DETAILS OF THE PRESSURE CORRECTION SCHEME

As stated in the main text, we apply a pressure correction scheme[8,9] to the constrained parametrizations. We add a small linear perturbation to the two-body FM potential:

$$\Delta U_{\mathrm{PC}} = -A\left(1 - \frac{r}{r_{\mathrm{cut}}}\right), \quad r_{\mathrm{cut}} = 1.2\,\mathrm{nm}. \tag{IV.1}$$

The constants A have to be adjusted for each interaction parameter γ in order to shift shift the pressure of the total interaction potential (2-b FM+PC and 3-b Δf_{FM}) to zero. The numerical values of A in units of kcal/mol are shown in Tab. I.

V. TABULATED POTENTIAL FILES

As described in subsection I B and subsection 2.3 of the main text, we employ cubic splines to represent the nonbonded pair potentials and the angular part of the SW potential $f^{(3b)}(\theta)$ in the FM procedure. This results in tabulated potential files which are used in LAMMPS to run the CG simulations with the pair style table (pair potentials) and the new pair style sw/table (SW parameters and angular potentials). The corresponding files for the interaction parameter $\gamma = 0.08\,\mathrm{nm}$ are:
"Methanol_2body_only_FM_pair_potential.txt": 2-body only FM of liquid methanol
"Methanol_2body_only_FM_PC_pair_potential.txt": 2-body only FM of liquid methanol with applied pressure correction. Has to be used togehter with the "Methanol_3body_FM_after_2body_FM_angular_potential.txt" angular potential.
"Methanol_2body_and_3body_together_FM_pair_potential.txt": concurrent 2-body and 3-body FM of liquid methanol pair potential
"Methanol_2body_and_3body_together_FM_angular_potential.txt": concurrent 2-body and 3-body FM of liquid methanol angular potential
"Methanol_3body_FM_after_2body_FM_angular_potential.txt": 2-body FM and 3-body Δf_{FM} of liquid methanol angular potential (pair potential is identical to 2-body only FM potential). If used together with the "Methanol_2body_only_FM_PC_p
pair potential this refers to the 2-body FM+PC and 3-body Δf_{FM} parametrization.
"Water_2body_only_FM_pair_potential.txt": 2-body only FM of liquid SPC/E water
"Water_2body_only_FM_PC_pair_potential.txt": 2-body only FM of liquid SPC/E with applied pressure correction. Has to be used togehter with the "Water_3body_FM_after_2body_FM_angular_potential.txt" angular potential.
"Water_2body_and_3body_together_FM_pair_potential.txt": concurrent 2-body and 3-body FM of liquid SPC/E water pair potential

"Water_2body_and_3body_together_FM_angular_potential.txt": concurrent 2-body and 3-body FM of liquid SPC/E water angular potential
"Water_3body_FM_after_2body_FM_angular_potential.txt": 2-body FM and 3-body Δf_{FM} of liquid SPC/E water angular potential (pair potential is identical to 2-body only FM potential). If used together with the "Water_2body_only_FM_PC_pair_potential.txt" pair potential this refers to the 2-body FM+PC and 3-body Δf_{FM} parametrization.

REFERENCES

[1]A. P. Thompson, S. J. Plimpton, and W. Mattson, J. Chem. Phys. **131**, 154107 (2009).
[2]C. Caleman, P. J. van Maaren, M. Hong, J. S. Hub, L. T. Costa, and D. van der Spoel, J. Chem. Theory. Comput. **8**, 61 (2012).
[3]J. Lu, Y. Qiu, R. Baron, and V. Molinero, J. Chem. Theory. Comput. **10**, 4104 (2014).
[4]S. Plimton, J. Comput. Phys. **117**, 1 (1995).
[5]S. Nosé, Molecular Physics **52**, 255 (1984).
[6]W. G. Hoover, Phys. Rev. A **31**, 1695 (1985).
[7]W. Shinoda, M. Shiga, and M. Mikami, Phys. Rev. B **69** (2004).
[8]D. Reith, M. Pütz, and F. Müller-Plathe, Journal of computational chemistry **24**, 1624 (2003).
[9]V. Rühle, C. Junghans, A. Lukyanov, K. Kremer, and D. Andrienko, J. Chem. Theory. Comput. **5**, 3211 (2009).